Model Predictive Power Control Approach for Three-Phase Single-Stage Grid-Tied PV Module-Integrated Converter

Amir Moghadasi, *Student Member, IEEE,* Arman Sargolzaei, *Member, IEEE,* Arash Khalilnejad, *Student Member, IEEE,* Masood Moghaddami, *Student Member, IEEE,* and Arif Sarwat, *Senior Member, IEEE,*

***Abstract*—This paper presents the concept of the three-phase module-integrated converters (MICs) incorporated in grid-tied large-scale photovoltaic (PV) systems. The current-source converter (CSC) with dc voltage boost capability, namely single-stage power conversion system, is proposed for three-phase PV MIC system. A model predictive scheme with low switching frequency is designed to control the proposed topology in such a way that provides a certain amount of active and reactive power in steady-state operation and also provides a proper ratio of reactive power under transient conditions to meet the low voltage ride through (LVRT) regulations. To predict the future behavior of current control values and switching states, a discrete-time model of the MIC is developed in synchronous reference frame. It is demonstrated that the injected active and reactive power can be controlled using minimizing the cost function introduced in the predictive switching algorithm. The proposed structure is simulated in MATLAB/SIMULINK software. The results verify the desired performance of the proposed control scheme for exchanging of both active and reactive powers between the PV MIC and the grid within different operating conditions.**

***Index Terms*—Active and reactive control, current source converter (CSC), low voltage ride through (LVRT), module-integrated converter (MIC), model predictive control (MPC).**

I. Introduction

THE attempts to reduce the greenhouse gas emissions are promising the recent dramatic increase of installed photovoltaic (PV) capacity, predicted 25% growth over the next 10 years [1]. Practically, the grid-tied PV system architectures can be classified into three basic types: centralized inverter, string or multistring inverter, and the AC module-integrated converter (MIC) (also called microinverter) [2]. Among these, MIC concept has become the most recent method for grid-tied PV system development in the market and it will be a tendency for future solar PV deployment, due to its superior advantages such as the low cost of mass production, high efficiency, easier installation, and improved energy harvest [3].

The commercial PV MIC systems are widely used in single-phase distributed PV generation with a power rating range of 150−400 W and input dc voltage variation of 20−45 V. Since the low PV voltage needs to be boosted to match the utility grid voltage, several MIC topologies based on the number of the conversion stages and the design specifications have been studied and presented in the literature [2]–[6]. Although these proposed topologies have shown promising results for single-phase small-scale residential and commercial PV applications, three-phase small-scale PV MIC concept can be taken into consideration for large-size PV installations, considering the merits of solar systems based on micro-inverters.

Conventional systems for a large-size PV installation are based on centralized or string inverters. Recently, development of the three-phase MIC concept to large-size PV installations, is introduced where each MIC is integrated directly into each PV panel [3]. This architecture will reduce the cost per watt, improve system reliability, and eliminate the single-point failure. Assuming further expansion of the three-phase grid-tied MIC system into large-scale PV installations, it would be required for micro-inverters to be equipped with low voltage ride through (LVRT) capability in order to fulfill the upcoming requirements under fault conditions. The previously analyzed control schemes focused on LVRT enhancement of the voltage source converter (VSC)-based MIC systems which are mostly based on the concept of $d-q$ rotating synchronous reference frame with classical linear proportional−integral (PI) regulators and pulsewidth/space vector modulation (PWM/SVM) [7]–[9].

Unlike VSC, the LVRT improvement of current-source converters (CSCs) in low power ranges (up to 500W) especially in PV MIC system, is rarely studied in the literature [10], [11]. A single-stage CSC topology, compared with VSC-based configurations, provides the alternative way to achieve the dc voltage boost capability without additional stages, so that circuitry complexity and the overall system losses may be reduced, as discussed in [11].

Recently, the finite control set model predictive control (FCS-MPC) has been used in many power electronic applications, due to the fact that it is simple intuitive method and can remove the need for linear regulators and modulation stages [12]–[14]. One of the advantages of MPC approach is that system nonlinearities and limitations can be incorporated directly into the model, resulting in better steady-state results and a faster transient response compared with classical controllers. The FCS-MPC method for the LVRT enhancement of the grid-tied VSC topology was previously studied in [13] and [14]. However, the power control of the CSC-based MIC using FCS-MPC strategy was not analyzed.

This paper develops the application of the single-stage CSC topology for the three-phase grid-tied PV MIC system. A predictive control strategy is applied to the CSC-based MIC to provide balanced grid currents under disturbances, simul-

A. Moghadasi, Arash Khalilnejad, Masood Moghaddami, and A. I. Sarwat are with the Department of Electrical and Computer Engineering, Florida International University, Miami, FL, USA (e-mail: amogh004@fiu.edu, asarwat@fiu.edu).

Arman Sargolzaei is with Department of Electrical Engineering, Polytechnique Florida university, Lakeland, FL, USA.

978-1-4799-8397-1/16/$31.00 © 2016 IEEE

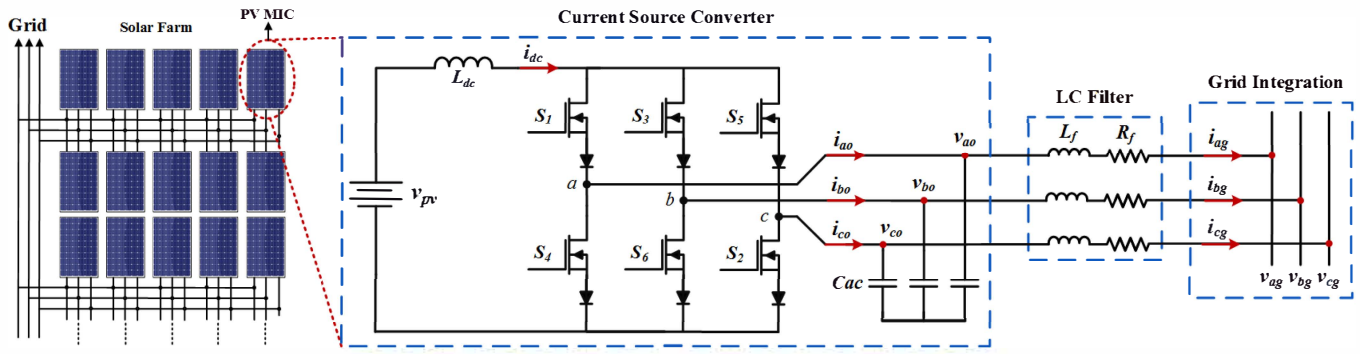

Fig. 1. Three-phase current source microinverter-based architecture for solar farm.

taneously with suitable active and reactive power regulation, allowing to fully meet the LVRT requirement. For this purpose, the system modeling is first presented in continuous-time and then converted to discrete-time models for the purpose of digital implementation. The control objectives are expressed as a fitness function. During each sampling interval, the fitness function is minimized using the actual measurements and predicted values for given switching states, which are then applied to the CSC-based MIC directly.

II. Configuration and Modeling of the CSC-Based MIC System

The system architecture for PV solar farm based on three-phase MICs is shown in Fig. 1. A three-phase CSC-based MIC is integrated directly into each panel. The outputs of each MIC are directly connected to low voltage three-phase grid, where each MIC operates independently regardless of the failure of other MICs. The proposed circuit is consist of a bridge with six reverse blocking MOSFET switches ($S_1 - S_6$) in series with a diode, a dc-link inductor L_{dc} as the main energy storage component, a dc-voltage source representing the output voltage of the PV arrays. The CSC is well suitable for MOSFETs since their inherent body diodes are inactive during commutation. The system connected to the three phase grid voltages v_{ag}, v_{bg}, v_{cg} through a high frequency LC filter.

A. Continuous-Time Modeling of CSC-Based MIC

In this paper, active power and reactive power are considered to be controlled by using the grid currents modeling presented in synchronous reference frame. For a three-phase CSC, 9 switching combinations, i.e., three charging operating modes and six discharging operating modes, are available as given in Table I. At any switching instant, only two active switches conduct, one of the upper MOSFETs (S_1, S_3, S_5) and one of the lower MOSFETs (S_4, S_6, S_2) to keep a flow pass for the inductor current, i_{dc}. The dc-link current conducting of the 9 possible switching states for the CSC-based MIC is shown in Fig. 2.

The $d-q$ components of the grid current can be expressed in terms converter output voltages, grid voltages and filter impedance as

$$\begin{cases} L_f \frac{di_{dg}}{dt} + R_f i_{dg} - L_f \omega_g i_{qg} = v_{do} - v_{dg} \\ L_f \frac{di_{qg}}{dt} + R_f i_{qg} + L_f \omega_g i_{dg} = v_{qo} - v_{qg} \end{cases} \quad (1)$$

TABLE I
Switching Combinations of the CSC-based MIC System

SC#	S_1	S_2	S_3	S_4	S_5	S_6	$i_{a\bullet}$	$i_{b\bullet}$	$i_{c\bullet}$
1	1	0	0	1	0	0	0	0	0
2	1	0	0	0	0	1	i_{dc}	$-i_{dc}$	0
3	1	1	0	0	0	0	i_{dc}	0	$-i_{dc}$
4	0	0	1	0	0	1	0	0	0
5	0	1	1	0	0	0	0	i_{dc}	$-i_{dc}$
6	0	0	1	1	0	0	$-i_{dc}$	i_{dc}	0
7	0	1	0	0	1	0	0	0	0
8	0	0	0	1	1	0	$-i_{dc}$	0	i_{dc}
9	0	0	0	0	1	1	0	$-i_{dc}$	i_{dc}

where, L_f and R_f represent grid filter inductance and its resistance, respectively. v_{do}, v_{qo}, v_{dg}, and v_{qg} are $dq-$axis converter and grid voltages, respectively. i_{dg}, i_{qg}, and ω_g are $dq-$axis grid currents and grid angular frequency, respectively.

The capacitor currents can be derived using converter output voltages as $i_{dc} = -\omega_g C_f v_{qo}$ and $i_{qc} = \omega_g C_f v_{do}$. Thus, the relationship between the converter output voltages and currents can be written in $dq-$axis shown as

$$\begin{cases} v_{do} = \frac{1}{\omega_g C_f}(i_{qo} - i_{qg}) \\ v_{qo} = \frac{1}{\omega_g C_f}(i_{dg} - i_{do}) \end{cases} \quad (2)$$

By combining the dynamic equations in (1) and (2), the continuous-time system describing the dq-axis grid currents can be obtained as

$$\frac{d}{dt}\begin{bmatrix} i_{dg} \\ i_{qg} \end{bmatrix} = \mathbf{A}\begin{bmatrix} i_{dg} \\ i_{qg} \end{bmatrix} + \mathbf{B}\begin{bmatrix} i_{do} \\ i_{qo} \end{bmatrix} + \mathbf{C}\begin{bmatrix} v_{dg} \\ v_{qg} \end{bmatrix} \quad (3)$$

where

$$\mathbf{A} = \begin{bmatrix} \frac{-R_f}{L_f} & \frac{\omega_g^2 L_f C_f - 1}{\omega_g L_f C_f} \\ \frac{-\omega_g^2 L_f C_f + 1}{\omega_g L_f C_f} & \frac{-R_f}{L_f} \end{bmatrix} \quad (4)$$

$$\mathbf{B} = \begin{bmatrix} 0 & \frac{1}{\omega_g L_f C_f} \\ \frac{-1}{\omega_g L_f C_f} & 0 \end{bmatrix}, \quad \mathbf{C} = \begin{bmatrix} \frac{-1}{L_f} & 0 \\ 0 & \frac{-1}{L_f} \end{bmatrix} \quad (5)$$

B. Discrete-Time Modeling of CSC-Based MIC

For the digital implementation of FCS-MPC algorithm, a discrete-time model of the system is needed. Microprocessor-based hardware helps in the real-time implementation of such models. Thus, in this section, all the continuous-time systems are converted to the discrete-time domain.

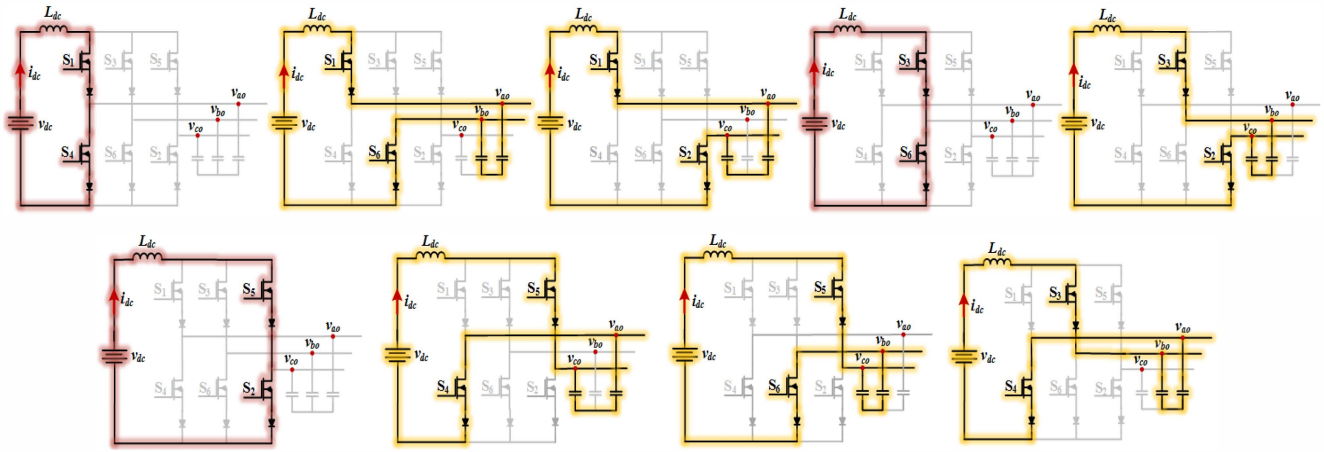

Fig. 2. The charging and discharging states of operation for CSC-based MIC.

The discrete-time system describing the $dq-$axis of the grid currents can be obtained from (3) for the one-step prediction as follows

$$\begin{bmatrix} i^p_{dg}(k+1) \\ i^p_{qg}(k+1) \end{bmatrix} = \mathbf{X_A} \begin{bmatrix} i_{dg}(k) \\ i_{qg}(k) \end{bmatrix} + \mathbf{X_B} \begin{bmatrix} i^e_{do}(k) \\ i^e_{qo}(k) \end{bmatrix} + \mathbf{X_C} \begin{bmatrix} v_{dg}(k) \\ v_{qg}(k) \end{bmatrix} \tag{6}$$

$$\mathbf{X_A} = e^{\mathbf{A}T_s},\ \mathbf{X_B} = \mathbf{A}^{-1}(\mathbf{X_A} - \mathbf{I})\mathbf{B},\ \mathbf{X_C} = \mathbf{A}^{-1}(\mathbf{X_A} - \mathbf{I})\mathbf{C} \tag{7}$$

where $i_{dg}(k)$, $i_{qg}(k)$, $v_{dg}(k)$, and $v_{qg}(k)$ are the $dq-$axis of the measured grid currents and voltages while T_s is controller sampling time.

The discrete values of the converter output currents in $dq-$axis reference frame can be estimated from switching signals $S_1(k) - S_6(k)$ and dc-link inductance current measurement, $i^m_{dc}(k)$, as express below:

$$\begin{bmatrix} i^e_{do}(k) \\ i^e_{qo}(k) \end{bmatrix} = \mathbf{K}.\langle i^m_{dc}(k) \begin{bmatrix} S_1(k) - S_4(k) \\ S_3(k) - S_6(k) \\ S_5(k) - S_2(k) \end{bmatrix} \rangle \tag{8}$$

where $\mathbf{K}$ is the abc/dq transformation matrix as:

$$\frac{2}{3} \begin{bmatrix} \cos\theta_g(k) & \cos(\theta_g(k) - \frac{2\pi}{3}) & \cos(\theta_g(k) - \frac{4\pi}{3}) \\ -\sin\theta_g(k) & -\sin(\theta_g(k) - \frac{2\pi}{3}) & -\sin(\theta_g(k) - \frac{4\pi}{3}) \end{bmatrix} \tag{9}$$

where $\theta_g(k)$ is grid voltage angle, which can be obtained by an phase-locked loop (PLL).

The one-step prediction methodology is often used to simplify analysis and digital implementation computations. However in the real-time implementation, the computational delay produced by the digital signal processor needs taking consideration [14]. Thus, the discrete time equation (6) is shifted one step forward, i.e., $(k+2)$ prediction.

To save computational effort, the same estimated converter currents $i^e_{do}(k)$ and $i^e_{qo}(k)$, are used in $(k+2)$ prediction of grid currents [14]. The discrete-time model for the two-step prediction of grid currents is as follows:

$$\begin{bmatrix} i^p_{dg}(k+2) \\ i^p_{qg}(k+2) \end{bmatrix} = \mathbf{X_A} \begin{bmatrix} i^p_{dg}(k+1) \\ i^p_{qg}(k+1) \end{bmatrix} + \mathbf{X_B} \begin{bmatrix} i^e_{do}(k) \\ i^e_{qo}(k) \end{bmatrix} + \mathbf{X_C} \begin{bmatrix} v_{dg}(k+1) \\ v_{qg}(k+1) \end{bmatrix} \tag{10}$$

where $i^p_{dg}(k+2)$ and $i^p_{qg}(k+2)$ are the predicted grid currents in $(k+2)$ state using 9 possible switching combinations. For a small enough sampling time and to save computational efforts, it is possible to consider $v_{dg}(k+1) \approx v_{dg}(k)$ and $v_{qg}(k+1) \approx v_{qg}(k)$.

From (6)–(10), the future behavior of the d-q components of the grid current which are related to the converter switching signals can be obtained based on the actual measurements and estimated converter currents. The optimal selection of a switching state among the 9 switching combinations leads to the proper regulation of the active and the reactive power of the PV MIC system.

III. Control System for the CSC-Based MIC

The FCS-MPC is an optimization control strategy, since it applies the optimized switching state directly to the converter, without using complex modulation techniques such as pulsewidth/space vector modulation (PWM/SVM). The proposed control system of the CSC-based MIC provides a certain amount of active and reactive power in steady-state operation and also a proper ratio of reactive power for LVRT regulations in transient-state operation. Detail of the proposed control scheme for the CSC-based MIC is illustrated in Fig. 3, which is schematically divided into two main blocks, i.e., command control generation block and model predictive current control block.

A. Generation of Reference Control Variables

In this section, the generation of reference control variables during steady-state and transient-state operation is presented. The $dq-$axis grid current references are generated by a method similar to the classical voltage-oriented control.

1) Steady-State Operation: in this operation mode, the control objectives for the CSC-based MIC include the following: 1) tracking of the reference dc-link current and 2) providing a certain amount of active and reactive power. Thus, through the PI controller-based regulation of the dc-link current, the $d-$axis grid reference current is generated. Assuming the maximum

978-1-4799-8397-1/16/$31.00 © 2016 IEEE

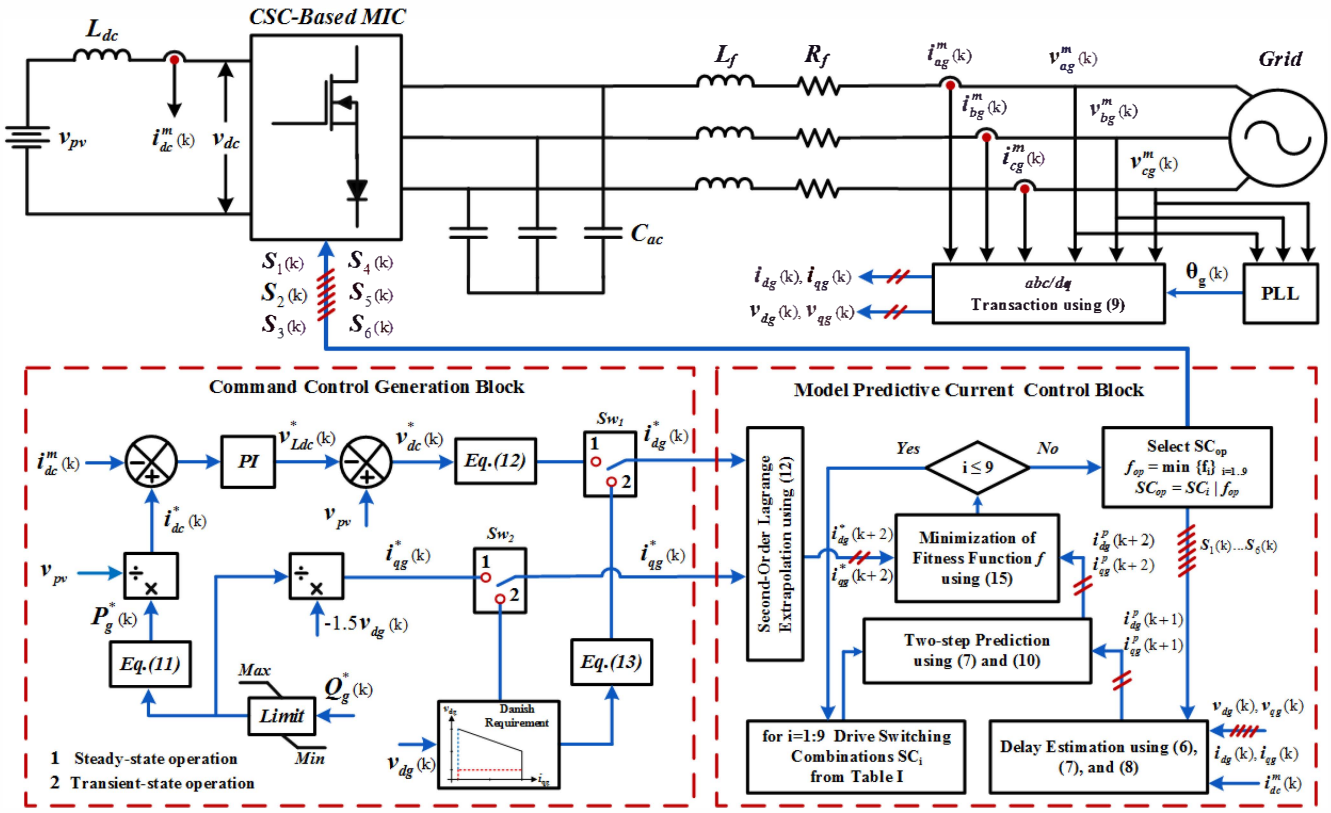

Fig. 3. Block diagram of the proposed control system for CSC-based MIC.

steady-state operating current at the grid terminal is 1 per unit (p.u.), the grid command active power can be derived, as follow

$$P_g^*(k) = \sqrt{S_{MIC}^2 - Q_g^*(k)^2} \tag{11}$$

where S_{MIC} is the rated power of the CSC-based MIC (300 VA in this paper).

The dc-link current reference, $i_{dc}^*(k)$ is extracted with the $P_g^*(k)$ command. Then, $i_{dc}^*(k)$ is compared with the measured dc-link current $i_{dc}^m(k)$ and error is given to the PI regulator to generate reference for v_{Ldc}^*. The dc voltages of the PV side and converter side, and the voltage across the dc-link inductance satisfy the equation $v_{Ldc}^*(k) = v_{pv} - v_{dc}^*(k)$. Neglecting the loss in the system ($P_g^* = P_{dc}^*$), grid active current $i_{dg}^*(k)$ is derived based on the power-balance assumption

$$i_{dg}^*(k) = \frac{P_g^*(k)}{1.5 v_{dg}(k)} = \frac{v_{dc}^*(k) i_{dc}(k)}{1.5 v_{dg}(k)} \tag{12}$$

The $q-$axis grid reference current $i_{qg}^*(k)$ can be simply obtained using $Q_g^*(k)$ command. Since ac-side capacitor C_{ac} injects a fixed amount of the reactive power to the grid, $Q_g^*(k)$ is limited by the maximum and minimum values.

2) Transient-State Operation: Recently, many power system operators are expanding and modifying their interconnection regulations such as LVRT requirements for large PV installations through the technical standard. A practical example of the LVRT requirements defined by the Danish system operator (Energinet. dk) is presented in [15]. Based on this regulation, the Sw_1 and Sw_2 are switched from position 1 to position 2 (see Fig.3) when the grid voltage falls below 90% of its nominal value. For the grid voltages in the range of 50%−90%, the PV MIC system should provide 2% reactive current for each 1% voltage dip, and once the grid voltage falls below 50%, the system should provide 100% reactive current. Assuming the rated rms phase current at the grid terminal is I_n, the $q-$component of the grid current in transient-state mode can be derived, as follow

$$i_{dg}^*(k) = \sqrt{I_n^2 - i_{qg}^*(k)^2} \tag{13}$$

B. Model Predictive Current Control Design

The proposed MPC scheme using two-step prediction strategy is shown in Fig. 3. The future value of the grid current in $(k+2)$ state is predicted among the 9 switching combinations generated by the CSC-based MIC, using (6) and (10).

An estimation of the current reference for the instant $k+2$, is needed for the predictive control strategy. Thus, the references obtained in kth instant (command control generation block) are extrapolated to $k+2$ instant. For the small sampling time, $T_s < 20\mu s$, it is reasonable to consider $i_g^*(k+2) = i_g^*(k)$. However, for T_s greater than $20\mu s$, the following second-order Lagrange extrapolation [13] can be used as

$$i_g^*(k+2) = 6i_g^*(k) - 8i_g^*(k-1) + 3i_g^*(k-2). \tag{14}$$

The predicted grid currents $i_{dg}^p(k+2)$ and $i_{qg}^p(k+2)$ are compared with their reference values $i_{dg}^*(k+2)$ and $i_{qg}^*(k+2)$, in a $d-q$ reference frame using a fitness function f, as follows

$$f = \| i_{dg}^*(k+2) - i_{dg}^p(k+2) \|^2 + \| i_{qg}^*(k+2) - i_{qg}^p(k+2) \|^2 \tag{15}$$

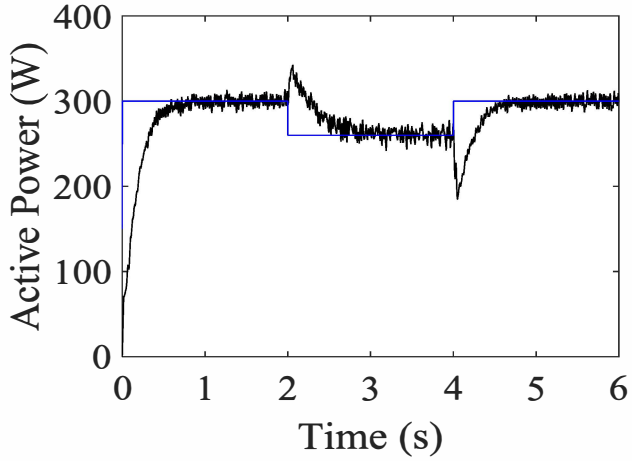

Fig. 4. The charging and discharging states of operation for CSC-based MIC.

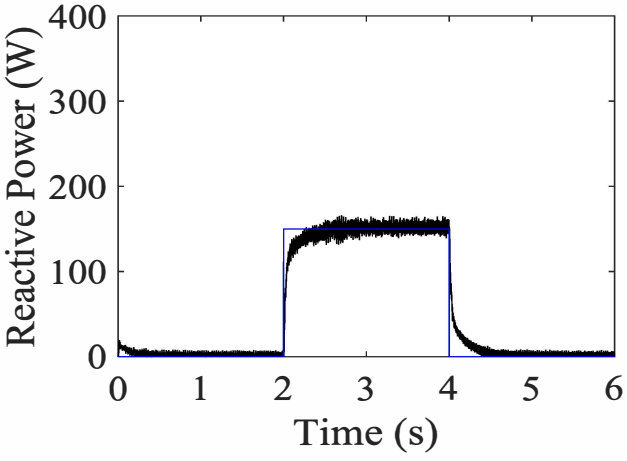

Fig. 5. The charging and discharging states of operation for CSC-based MIC.

The goal of the fitness function optimization is to achieve the f value close to zero. With this approach, the best switching state in the previous iteration is used to estimate the control variables at $(k+1)$ instant. The prediction of $(k+2)$ variables is carried out using all the switching combinations from Table I. The switching state which minimizes the fitness function at $(k+2)$ instant is chosen and then applied to CSC-based MIC at the next sampling instant.

IV. Simulation Results

The result of the simulation performed by MATLAB-Simulink is presented in this section to show the effectiveness of the proposed control method. The systems rated power is 300 VA with voltage and frequency of 120 V and 60 Hz, respectively. The DC link voltage is 50 V and the circuit parameters for the simulation are selected as: C_f=15 μF, L_f=2 mH, R_f= 2 Ω, R_{dc}=0.2 Ω, and L_{dc}=6 mH. The set value of the switching frequency is 2 kHz.

To observe the operation of the control system, the step response is analyzed. The dynamic response of the active and reactive power to step changes in reference active and reactive power in no fault condition is shown in Figs. 4 and 5. Active reference power changes from 300 W to 260 W at t=2s and returns to its initial value at t = 4s. In the meantime, the reference reactive power goes to 150 Var and then gets back to zero. At the time of variation, the sudden increase in reactive power causes the active power to increase, then it stabilize at the reference value. Also, when the reference gets back to 300 W, due to sudden decrease in reactive power, active power has reverse spike, then follows the reference power. It should be mentioned that the smoother the change in the reactive power, the less spike occurs in the active power, and on the other hand, takes more time to stabilize.

Also, the operation of the system is analyzed in fault condition. At t = 2s, fault occurs and active power reference drops to zero. At t = 2.2s the fault is cleared and active reference power gets back to 300 W. While at the mentioned interval the reactive power reference raises to 300 W and gets back to zero. As can be seen in Figs. 6 and 7, the reactive power change in fault time does not let the active power to drop to zero. The time duration of fault is not that much to let to reactive power to increase to the reference amount of 300 Var. Along with the return of the reactive power to zero, the active power gets back 300 W.

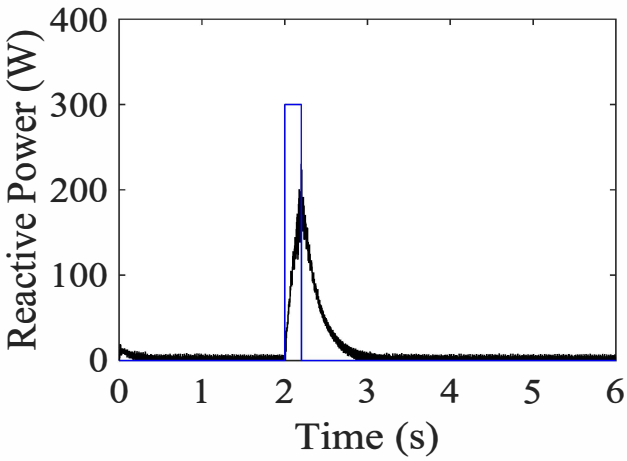

Fig. 6. The charging and discharging states of operation for CSC-based MIC.

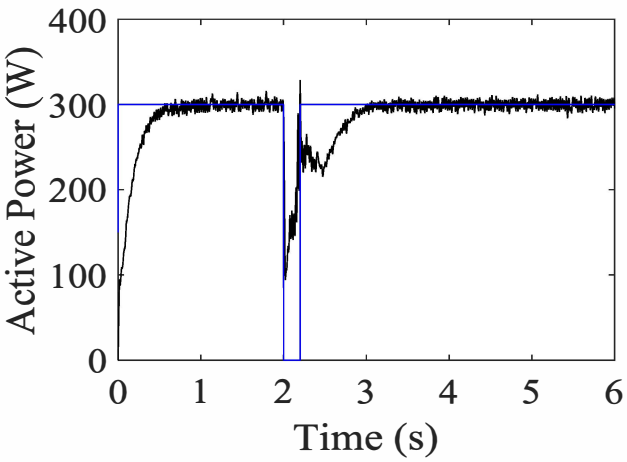

Fig. 7. The charging and discharging states of operation for CSC-based MIC.

V. Conclusion

In this paper, the 300-VA single-stage three-phase CSC was proposed and implemented as a promising solution for MICs in grid-tied large-scale PV systems. A model predictive control scheme is proposed independently control the active and reactive powers exchanging between the PV and the utility grid in order to meet recent grid-code and LVRT requirements. The PPWM switching technique for CSC topology was formulated based on the voltage phasor quantities. It is demonstrated that the injected active and reactive power can be regulated through modulation index m_i and the modulation angle a_0, introduced into the PPWM switching algorithm. The proposed control method was verified in simulation. The results showed fast transient response and good stability which indicate the effectiveness and robustness of the proposed control scheme.

References

[1] R. Singh, G. Alapatt, and A. Lakhtakia, "Making solar cells a reality in every home: Opportunities and challenges for photovoltaic device design," *Electron Devices Society, IEEE Journal of the*, vol. 1, no. 6, pp. 129–144, June 2013.

[2] Q. Li and P. Wolfs, "A review of the single phase photovoltaic module integrated converter topologies with three different dc link configurations," *Power Electronics, IEEE Transactions on*, vol. 23, no. 3, pp. 1320–1333, May 2008.

[3] L. Chen, A. Amirahmadi, Q. Zhang, N. Kutkut, and I. Batarseh, "Design and implementation of three-phase two-stage grid-connected module integrated converter," *Power Electronics, IEEE Transactions on*, vol. 29, no. 8, pp. 3881–3892, Aug 2014.

[4] S. Kjaer, J. Pedersen, and F. Blaabjerg, "A review of single-phase grid-connected inverters for photovoltaic modules," *Industry Applications, IEEE Transactions on*, vol. 41, no. 5, pp. 1292–1306, Sept 2005.

[5] F. Z. Peng, "Z-source inverter," *Industry Applications, IEEE Transactions on*, vol. 39, no. 2, pp. 504–510, Mar 2003.

[6] Y. Zhou, L. Liu, and H. Li, "A high-performance photovoltaic module-integrated converter (mic) based on cascaded quasi-z-source inverters (qzsi) using egan fets," *Power Electronics, IEEE Transactions on*, vol. 28, no. 6, pp. 2727–2738, June 2013.

[7] F. Blaabjerg, R. Teodorescu, M. Liserre, and A. Timbus, "Overview of control and grid synchronization for distributed power generation systems," *Industrial Electronics, IEEE Transactions on*, vol. 53, no. 5, pp. 1398–1409, Oct 2006.

[8] M. Liserre, R. Teodorescu, and F. Blaabjerg, "Multiple harmonics control for three-phase grid converter systems with the use of pi-res current controller in a rotating frame," *Power Electronics, IEEE Transactions on*, vol. 21, no. 3, pp. 836–841, May 2006.

[9] M. Castilla, J. Miret, J. Matas, L. Garcia de Vicuna, and J. Guerrero, "Control design guidelines for single-phase grid-connected photovoltaic inverters with damped resonant harmonic compensators," *Industrial Electronics, IEEE Transactions on*, vol. 56, no. 11, pp. 4492–4501, Nov 2009.

[10] B. Sahan, A. Vergara, N. Henze, A. Engler, and P. Zacharias, "A single-stage pv module integrated converter based on a low-power current-source inverter," *Industrial Electronics, IEEE Transactions on*, vol. 55, no. 7, pp. 2602–2609, July 2008.

[11] Y. Chen and K. Smedley, "Three-phase boost-type grid-connected inverter," *Power Electronics, IEEE Transactions on*, vol. 23, no. 5, pp. 2301–2309, Sept 2008.

[12] V. Yaramasu, M. Rivera, B. Wu, and J. Rodriguez, "Model predictive current control of two-level four-leg inverters-part i: Concept, algorithm, and simulation analysis," *IEEE Transactions on Power Electronics*, vol. 28, no. 7, pp. 3459–3468, July 2013.

[13] A. Calle-Prado, S. Alepuz, J. Bordonau, J. Nicolas-Apruzzese, P. Corts, and J. Rodriguez, "Model predictive current control of grid-connected neutral-point-clamped converters to meet low-voltage ride-through requirements," *IEEE Transactions on Industrial Electronics*, vol. 62, no. 3, pp. 1503–1514, March 2015.

[14] V. Yaramasu, B. Wu, S. Alepuz, and S. Kouro, "Predictive control for low-voltage ride-through enhancement of three-level-boost and npc-converter-based pmsg wind turbine," *IEEE Transactions on Industrial Electronics*, vol. 61, no. 12, pp. 6832–6843, Dec 2014.

[15] A. Moghadasi, A. Sarwat, and J. Guerrero, "A comprehensive review of low-voltage-ride-through methods for fixed-speed wind power generators," *Renewable and Sustainable Energy Reviews*, vol. 55, pp. 823–839, March 2016.

978-1-4799-8397-1/16/$31.00 © 2016 IEEE